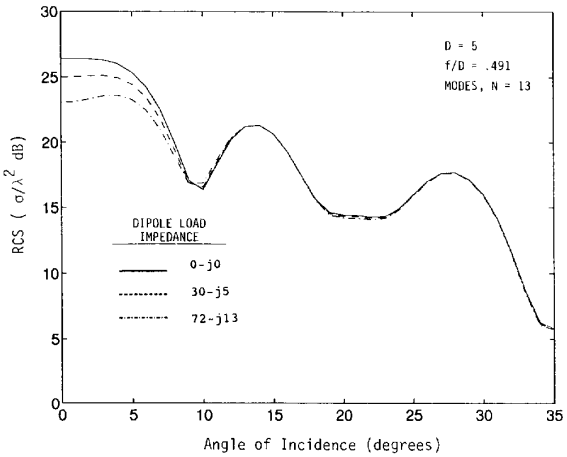

Fig. 5. Computed RCS for a reflector with a cavity-backed dipole feed at a threat frequency in the antenna operating band. (Feed dimensions are twice those shown in Fig. 1.)

Fig. 1 could not be scaled up by a factor of 2 along with the feed. However, Fig. 5 shows the in-band RCS of the feed with a 5λ reflector ($f/D = 0.491$), which clearly identifies the load contribution.

IV. Conclusions

A method of moments solution for the scattering from a parabolic reflector antenna with a cavity-backed dipole feed has been presented. The solution is valid at any frequency, but because of the need to include a large number of azimuthal modes for convergence, the memory requirements are severe. At low out-of-band frequencies, the dipole is not a significant contributor to the total RCS. To reduce the computer run time the dipole can be neglected, in which case the azimuthal modes become independent and each of the diagonal blocks of Z can be inverted separately. At threat frequencies in the operating band of the antenna, the dipole contribution is significant, but only at angles near boresight ($\theta = 0°$).

References

[1] J. R. Mautz and R. F. Harrington, "An improved E-field solution for a conducting body of revolution," Tech. Rep. TR-80–1, Syracuse University.

[2] J. F. Shaeffer and L. N. Medgyesi-Mitschang, "Radiation from wire antennas attached to bodies of revolution: The junction problem," *IEEE Trans. Antennas Propagat.*, vol. 29, p. 479, May 1981.

[3] J. E. Fletcher, "Radar cross section of reflector antennas," master's thesis, Naval Postgraduate School, June 1992 (limited distribution).

[4] W. V. T. Rusch, "A comparison of geometrical and integral fields from high-frequency reflectors," *Proc. IEEE*, vol. 62, p. 1603, Nov. 1974.

[5] R. C. Hansen, "Relationship between antennas as scatterers and as radiators," *Proc. IEEE*, vol. 77, p. 659, May. 1989.

The Finite-Difference Time-Domain Method Applied to Anisotropic Material

John Schneider and Scott Hudson

***Abstract*— The finite-difference time-domain (FDTD) method has received considerable attention recently. The popularity of this method stems from the fact that it is not limited to a specific geometry and it does not restrict the constitutive parameters of a scatterer. Furthermore, it provides a direct solution to problems with transient illumination, but can also be used for harmonic analysis. However, researchers have limited their investigations to materials that are either isotropic or that have diagonal permittivity, conductivity, and permeability tensors. In this paper, we derive the necessary extension to the FDTD equations to accommodate nondiagonal tensors. Excellent agreement between FDTD and exact analytic results is obtained for a one-dimensional anisotropic scatterer.**

I. Introduction

The finite-difference time-domain (FDTD) method was first proposed by Yee [1] as a direct solution of Maxwell's time-domain curl equations. In this algorithm, one begins by making a judicious discretization of space-time. The temporal and spatial derivatives in Maxwell's curl equations are then approximated by difference equations, and, finally, the resulting difference equations are solved for the fields at the "next" time step in terms of values at "previous" time steps. In this manner, a leapfrog algorithm is used to obtain the fields for all space-time given the incident field and knowledge of the fields throughout space at some initial time. Taflove and Brodwin later developed the correct stability criterion for FDTD [2]. Since then, Taflove and his colleagues, as well as many others, have produced a large body of literature covering many applications of and enhancements to the FDTD algorithm (for a survey, see [3]). Part of the success of FDTD is due to the development of absorbing boundary conditions (ABC's) that absorb energy propagating from the interior to the edge of the computational mesh. Currently, two of the more popular ABC's are those of Mur [4] and Liao [5], [6].

The majority of FDTD applications have assumed scattering from or propagation through a material that is both nondispersive and isotropic. Recently, Luebbers *et al.* developed an algorithm for frequency-dependent materials [7], called $(FD)^2TD$, which was used to obtain the reflection coefficients from plasma layers [8]. Nickisch and Franke [9] have also developed an FDTD algorithm for dispersive materials. Taflove and Umashankar [10], Beker *et al.* [11], and Strikel and Taflove [12] have published results using FDTD with anisotropic materials. However, their work has been restricted to materials with diagonal tensors, and the resulting equations are nearly identical to those used in the original Yee algorithm. As will be shown, off-diagonal terms produce coupling of temporal derivatives in the curl equations and the resulting difference equations are considerably different from the diagonal-tensor case.

We are interested in accurately modeling scattering from composite materials such as those used in the construction of modern aircraft and automobiles. These materials often have embedded carbon fibers that produce a high conductivity in a particular direction and hence are anisotropic. If sheets of this type of material are sandwiched together

Manuscript received November 2, 1992; revised February 4, 1993.

The authors are with the School of Electrical Engineering and Computer Science, Washington State University, Pullman, WA 99164-2752.

IEEE Log Number 9211268.

and the fibers in each sheet are not parallel and/or orthogonal, it is impossible to model the material with diagonal tensors. Instead, the off-diagonal elements of the tensor must be accommodated.

In this paper, we outline the steps needed to obtain the FDTD time-stepping equations for a general three-dimensional anisotropic scatterer. The simplified equations for a one-dimensional scatterer are then examined. We use these equations to obtain the reflection coefficients for a layered material that consists of three slabs of an anisotropic material. Excellent agreement is shown between FDTD and exact analytic results.

II. FDTD FOR ANISOTROPIC MATERIAL

In anisotropic material, the electric flux density is related to the electric field by a permittivity tensor, $\mathbf{D} = \overline{\overline{\epsilon}}\mathbf{E}$, which can be written as

$$\begin{bmatrix} D_x \\ D_y \\ D_z \end{bmatrix} = \begin{bmatrix} \epsilon_{xx} & \epsilon_{xy} & \epsilon_{xz} \\ \epsilon_{yx} & \epsilon_{yy} & \epsilon_{yz} \\ \epsilon_{zx} & \epsilon_{zy} & \epsilon_{zz} \end{bmatrix} \begin{bmatrix} E_x \\ E_y \\ E_z \end{bmatrix}. \tag{1}$$

Similarly, the conduction current and electric field are related through a conductivity tensor, $\mathbf{J} = \overline{\overline{\sigma}}\mathbf{E}$. We will restrict ourselves to nonmagnetic materials so that the magnetic flux density and the magnetic field are related by $\mathbf{B} = \mu_0\mathbf{H}$, where μ_0 is the permeability of free space. For this case, Maxwell's curl equations are

$$\nabla \times \mathbf{E} = -\mu_0 \frac{\partial \mathbf{H}}{\partial t}, \tag{2}$$

$$\nabla \times \mathbf{H} = \overline{\overline{\sigma}}\mathbf{E} + \overline{\overline{\epsilon}}\frac{\partial \mathbf{E}}{\partial \mathbf{t}}. \tag{3}$$

The FDTD algorithm assumes that space is discretized so that each field quantity is available only at a unique location. These locations are given by the Yee cell shown in Fig. 1. The Yee cell specifies the spatial location where each field is available, but it is further assumed that $\mathbf{E}$ is temporally available only at integer values of Δt, while $\mathbf{H}$ is available a half time step away. This discretization leads naturally to the following notation: assuming the argument (x, y, z, t) is evaluated at points $(i\Delta x, j\Delta y, k\Delta z, n\Delta t)$, the function $A(x, y, z, t)$ can be written $A|^n_{i,j,k}$. Initially, we will use the i, j, k spatial subscript as a "generic" index; i.e., it does not truly give the location where the field is evaluated. For example, in the following equation, the term $H_x|^{n+\frac{1}{2}}_{i,j,k}$ appears. However, referring to Fig. 1, H_x is not available at the location i, j, k but is found at $i, j+\frac{1}{2}, k+\frac{1}{2}$. Thus, when the fields are evaluated, the j and k indices must be increased by $+\frac{1}{2}$ throughout the equation. We will return to this issue after obtaining the needed difference equations.

An approximation to (2) can be obtained at the point $(i\Delta x, j\Delta y, k\Delta z, n\Delta t)$ by approximating the derivatives by difference equations; then the magnetic field at time $n+\frac{1}{2}$ can be obtained in terms of previously obtained quantities. For H_x we obtain

$$H_x|^{n+\frac{1}{2}}_{i,j,k} = H_x|^{n-\frac{1}{2}}_{i,j,k} + \frac{\Delta t}{\mu_0}\left\{\frac{1}{\Delta z}\left(E_y|^n_{i,j,k+\frac{1}{2}} - E_y|^n_{i,j,k-\frac{1}{2}}\right) - \frac{1}{\Delta y}\left(E_z|^n_{i,j+\frac{1}{2},k} - E_z|^n_{i,j-\frac{1}{2},k}\right)\right\}. \tag{4}$$

Similar equations can be obtained for H_y and H_z. Since it was assumed that the material was nonmagnetic, these equations are the same as those that apply to isotropic material and are given in any standard FDTD reference (e.g. [1]–[3]).

Separating (3) into scalar components yields the following three equations:

$$\frac{\partial H_z}{\partial y} - \frac{\partial H_y}{\partial z} = \sigma_{xx}E_x + \sigma_{xy}E_y + \sigma_{xz}E_z + \epsilon_{xx}\frac{\partial E_x}{\partial t} + \epsilon_{xy}\frac{\partial E_y}{\partial t} + \epsilon_{xz}\frac{\partial E_z}{\partial t}, \tag{5}$$

$$\frac{\partial H_x}{\partial z} - \frac{\partial H_z}{\partial x} = \sigma_{yx}E_x + \sigma_{yy}E_y + \sigma_{yz}E_z + \epsilon_{yx}\frac{\partial E_x}{\partial t} + \epsilon_{yy}\frac{\partial E_y}{\partial t} + \epsilon_{yz}\frac{\partial E_z}{\partial t}, \tag{6}$$

$$\frac{\partial H_y}{\partial x} - \frac{\partial H_x}{\partial y} = \sigma_{zx}E_x + \sigma_{zy}E_y + \sigma_{zz}E_z + \epsilon_{zx}\frac{\partial E_x}{\partial t} + \epsilon_{zy}\frac{\partial E_y}{\partial t} + \epsilon_{zz}\frac{\partial E_z}{\partial t}. \tag{7}$$

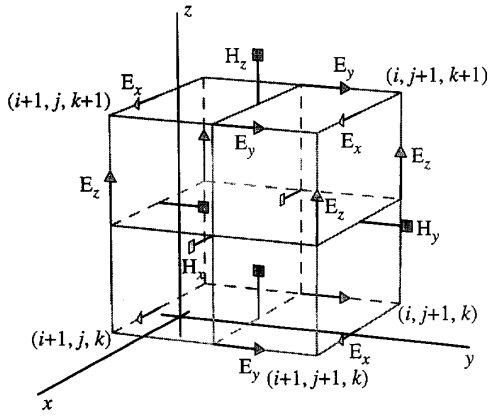

Fig. 1. The Yee cell used to determine the location of field evaluation points.

Note that the off-diagonal terms cause each of the three temporal derivatives of the electric field to appear on the right-hand side of these equations. When these terms vanish, the temporal derivatives decouple and the electric field at the next time step can be obtained in a simple manner from previous values as was done for the magnetic fields. We will consider $\mathbf{E}$ at the point $(i\Delta x, j\Delta y, k\Delta z, (n+\frac{1}{2})\Delta t)$. Even though the electric fields are not explicitly available at the time $n+\frac{1}{2}$, they may be approximated, for example, by

$$E_z|^{n+\frac{1}{2}}_{i,j,k} \approx \frac{1}{2}\left(E_z|^{n+1}_{i,j,k} + E_z|^n_{i,j,k}\right), \tag{8}$$

where similar approximations apply to E_x and E_y. The temporal derivatives may be approximated by

$$\frac{\partial E_z}{\partial t} \approx \frac{1}{\Delta t}\left(E_z|^{n+1}_{i,j,k} - E_z|^n_{i,j,k}\right). \tag{9}$$

Again, similar approximations apply to the derivatives of E_x and E_y. Using these discretizations, the x component of Ampere's law (5) can be written

$$\begin{aligned}\frac{\partial H_z}{\partial y}\Big|^{n+\frac{1}{2}}_{i,j,k} - \frac{\partial H_y}{\partial z}\Big|^{n+\frac{1}{2}}_{i,j,k} &= \left(\frac{\epsilon_{xx}}{\Delta t} + \frac{\sigma_{xx}}{2}\right)E_x|^{n+1}_{i,j,k} - \left(\frac{\epsilon_{xx}}{\Delta t} - \frac{\sigma_{xx}}{2}\right)E_x|^n_{i,j,k} + \left(\frac{\epsilon_{xy}}{\Delta t} + \frac{\sigma_{xy}}{2}\right)E_y|^{n+1}_{i,j,k} \\ &\quad - \left(\frac{\epsilon_{xy}}{\Delta t} - \frac{\sigma_{xy}}{2}\right)E_y|^n_{i,j,k} + \left(\frac{\epsilon_{xz}}{\Delta t} + \frac{\sigma_{xz}}{2}\right)E_z|^{n+1}_{i,j,k} \\ &\quad - \left(\frac{\epsilon_{xz}}{\Delta t} - \frac{\sigma_{xz}}{2}\right)E_z|^n_{i,j,k}.\end{aligned} \tag{10}$$

Similar expressions hold for the y and z components. In these expressions, only quantities at time step $n+1$ are unknown while all other values are either known explicitly or can be interpolated from other known values. These equations can be written in matrix form and solved for the electric field at the next time step. We obtain

$$\begin{bmatrix} E_x|_{i,j,k}^{n+1} \\ E_y|_{i,j,k}^{n+1} \\ E_z|_{i,j,k}^{n+1} \end{bmatrix} = \left(\frac{1}{\Delta t}\bar{\bar{\epsilon}} + \frac{1}{2}\bar{\bar{\sigma}}\right)^{-1} \left\{ \begin{bmatrix} \frac{\partial H_z}{\partial y}\Big|_{i,j,k}^{n+\frac{1}{2}} - \frac{\partial H_y}{\partial z}\Big|_{i,j,k}^{n+\frac{1}{2}} \\ \frac{\partial H_x}{\partial z}\Big|_{i,j,k}^{n+\frac{1}{2}} - \frac{\partial H_z}{\partial x}\Big|_{i,j,k}^{n+\frac{1}{2}} \\ \frac{\partial H_y}{\partial x}\Big|_{i,j,k}^{n+\frac{1}{2}} - \frac{\partial H_x}{\partial y}\Big|_{i,j,k}^{n+\frac{1}{2}} \end{bmatrix} + \left(\frac{1}{\Delta t}\bar{\bar{\epsilon}} - \frac{1}{2}\bar{\bar{\sigma}}\right) \begin{bmatrix} E_x|_{i,j,k}^{n} \\ E_y|_{i,j,k}^{n} \\ E_z|_{i,j,k}^{n} \end{bmatrix} \right\}. \tag{11}$$

Although the solution to this equation is rather cumbersome, it can be obtained in a straightforward manner. We will limit ourselves here to consideration of the E_z component.

$$\begin{aligned} E_z|_{i,j,k}^{n+1} = \frac{1}{\delta}\Bigg\{ & \left[\left(\frac{\epsilon_{xy}}{\Delta t} + \frac{\sigma_{xy}}{2}\right)\left(\frac{\epsilon_{zx}}{\Delta t} + \frac{\sigma_{zx}}{2}\right) - \left(\frac{\epsilon_{xx}}{\Delta t} + \frac{\sigma_{xx}}{2}\right)\left(\frac{\epsilon_{zy}}{\Delta t} + \frac{\sigma_{zy}}{2}\right)\right] \\ & \left[\left(\frac{\epsilon_{yx}}{\Delta t} - \frac{\sigma_{yx}}{2}\right) E_x|_{i,j,k}^{n} + \left(\frac{\epsilon_{yy}}{\Delta t} - \frac{\sigma_{yy}}{2}\right) E_y|_{i,j,k}^{n} + \left(\frac{\epsilon_{yz}}{\Delta t} - \frac{\sigma_{yz}}{2}\right) E_z|_{i,j,k}^{n} \right. \\ & \left. + \frac{\partial H_x}{\partial z}\Big|_{i,j,k}^{n+\frac{1}{2}} - \frac{\partial H_z}{\partial x}\Big|_{i,j,k}^{n+\frac{1}{2}}\right] \\ & + \left[\left(\frac{\epsilon_{yx}}{\Delta t} + \frac{\sigma_{yx}}{2}\right)\left(\frac{\epsilon_{zy}}{\Delta t} + \frac{\sigma_{zy}}{2}\right) - \left(\frac{\epsilon_{yy}}{\Delta t} + \frac{\sigma_{yy}}{2}\right)\left(\frac{\epsilon_{zx}}{\Delta t} + \frac{\sigma_{zx}}{2}\right)\right] \\ & \left[\left(\frac{\epsilon_{xx}}{\Delta t} - \frac{\sigma_{xx}}{2}\right) E_x|_{i,j,k}^{n} + \left(\frac{\epsilon_{xy}}{\Delta t} - \frac{\sigma_{xy}}{2}\right) E_y|_{i,j,k}^{n} + \left(\frac{\epsilon_{xz}}{\Delta t} - \frac{\sigma_{xz}}{2}\right) E_z|_{i,j,k}^{n} \right. \\ & \left. + \frac{\partial H_y}{\partial z}\Big|_{i,j,k}^{n+\frac{1}{2}} - \frac{\partial H_z}{\partial y}\Big|_{i,j,k}^{n+\frac{1}{2}}\right] \\ & + \left[\left(\frac{\epsilon_{xx}}{\Delta t} + \frac{\sigma_{xx}}{2}\right)\left(\frac{\epsilon_{yy}}{\Delta t} + \frac{\sigma_{yy}}{2}\right) - \left(\frac{\epsilon_{xy}}{\Delta t} + \frac{\sigma_{xy}}{2}\right)\left(\frac{\epsilon_{yx}}{\Delta t} + \frac{\sigma_{yx}}{2}\right)\right] \\ & \left[\left(\frac{\epsilon_{zx}}{\Delta t} - \frac{\sigma_{zx}}{2}\right) E_x|_{i,j,k}^{n} + \left(\frac{\epsilon_{zy}}{\Delta t} - \frac{\sigma_{zy}}{2}\right) E_y|_{i,j,k}^{n} + \left(\frac{\epsilon_{zz}}{\Delta t} - \frac{\sigma_{zz}}{2}\right) E_z|_{i,j,k}^{n} \right. \\ & \left. + \frac{\partial H_y}{\partial x}\Big|_{i,j,k}^{n+\frac{1}{2}} - \frac{\partial H_x}{\partial y}\Big|_{i,j,k}^{n+\frac{1}{2}}\right]\Bigg\} \end{aligned} \tag{12}$$

where δ is the determinant of the matrix $\left(\frac{1}{\Delta t}\bar{\bar{\epsilon}} + \frac{1}{2}\bar{\bar{\sigma}}\right)$. When the off-diagonal terms are zero, (12) reduces to the standard FDTD equation for E_z. As mentioned previously, the i, j, k indices used in the previous equations were not meant to give the true location where the fields are available. To implement these equations we must consider the actual locations of the field quantities. In the Yee cell (Fig. 1), electric field quantities are only found at the following locations:

$$E_x \text{ at } ((i+\frac{1}{2})\Delta x, j\Delta y, k\Delta z, n\Delta t), \tag{13}$$

$$E_y \text{ at } (i\Delta x, (j+\frac{1}{2})\Delta y, k\Delta z, n\Delta t), \tag{14}$$

$$E_z \text{ at } (i\Delta x, j\Delta y, (k+\frac{1}{2})\Delta z, n\Delta t). \tag{15}$$

Therefore, (12) would be used to find $E_z|_{i,j,k+\frac{1}{2}}^{n+1}$ which requires the use of $E_x|_{i,j,k+\frac{1}{2}}^{n}$, $E_y|_{i,j,k+\frac{1}{2}}^{n}$, $\frac{\partial H_x}{\partial z}\Big|_{i,j,k+\frac{1}{2}}^{n+\frac{1}{2}}$, $\frac{\partial H_y}{\partial z}\Big|_{i,j,k+\frac{1}{2}}^{n+\frac{1}{2}}$, $\frac{\partial H_z}{\partial x}\Big|_{i,j,k+\frac{1}{2}}^{n+\frac{1}{2}}$, and $\frac{\partial H_z}{\partial y}\Big|_{i,j,k+\frac{1}{2}}^{n+\frac{1}{2}}$, but these values are not available directly from the FDTD grid. Instead, they must be interpolated from neighboring quantities. Thus, the following approximations are used for E_x and E_y:

$$E_x|_{i,j,k+\frac{1}{2}}^{n} = \frac{1}{4}\left(E_x|_{i+\frac{1}{2},j,k+1}^{n} + E_x|_{i+\frac{1}{2},j,k}^{n} + E_x|_{i-\frac{1}{2},j,k+1}^{n} + E_x|_{i-\frac{1}{2},j,k}^{n}\right) \tag{16}$$

$$E_y|_{i,j,k+\frac{1}{2}}^{n} = \frac{1}{4}\left(E_y|_{i,j+\frac{1}{2},k+1}^{n} + E_y|_{i,j+\frac{1}{2},k}^{n} + E_y|_{i,j-\frac{1}{2},k+1}^{n} + E_y|_{i,j-\frac{1}{2},k}^{n}\right) \tag{17}$$

Magnetic field quantities are only found as follows:

$$H_x \text{ at } (i\Delta x, (j+\frac{1}{2})\Delta y, (k+\frac{1}{2})\Delta z, (n+\frac{1}{2})\Delta t) \tag{18}$$

$$H_y \text{ at } ((i+\frac{1}{2})\Delta x, j\Delta y, (k+\frac{1}{2})\Delta z, (n+\frac{1}{2})\Delta t) \tag{19}$$

$$H_z \text{ at } ((i+\frac{1}{2})\Delta x, (j+\frac{1}{2})\Delta y, k\Delta z, (n+\frac{1}{2})\Delta t) \tag{20}$$

Therefore, the spatial derivatives of the magnetic field can be obtained using the following approximations:

$$\left.\frac{\partial H_x}{\partial z}\right|_{i,j,k+\frac{1}{2}}^{n+\frac{1}{2}} = \frac{1}{4\Delta z}\left(H_x|_{i,j+\frac{1}{2},k+\frac{3}{2}}^{n+\frac{1}{2}} + H_x|_{i,j-\frac{1}{2},k+\frac{3}{2}}^{n+\frac{1}{2}} - H_x|_{i,j+\frac{1}{2},k-\frac{1}{2}}^{n+\frac{1}{2}} - H_x|_{i,j-\frac{1}{2},k-\frac{1}{2}}^{n+\frac{1}{2}}\right) \tag{21}$$

$$\left.\frac{\partial H_y}{\partial z}\right|_{i,j,k+\frac{1}{2}}^{n+\frac{1}{2}} = \frac{1}{4\Delta z}\left(H_y|_{i+\frac{1}{2},j,k+\frac{3}{2}}^{n+\frac{1}{2}} + H_y|_{i-\frac{1}{2},j,k+\frac{3}{2}}^{n+\frac{1}{2}} - H_y|_{i+\frac{1}{2},j,k-\frac{1}{2}}^{n+\frac{1}{2}} - H_y|_{i-\frac{1}{2},j,k-\frac{1}{2}}^{n+\frac{1}{2}}\right) \tag{22}$$

$$\begin{aligned}\left.\frac{\partial H_z}{\partial x}\right|_{i,j,k+\frac{1}{2}}^{n+\frac{1}{2}} = \frac{1}{4\Delta x}\Big(& H_z|_{i+\frac{1}{2},j+\frac{1}{2},k+1}^{n+\frac{1}{2}} + H_z|_{i+\frac{1}{2},j+\frac{1}{2},k}^{n+\frac{1}{2}} + H_z|_{i+\frac{1}{2},j-\frac{1}{2},k+1}^{n+\frac{1}{2}} + H_z|_{i+\frac{1}{2},j-\frac{1}{2},k}^{n+\frac{1}{2}} \\ & - H_z|_{i-\frac{1}{2},j+\frac{1}{2},k+1}^{n+\frac{1}{2}} - H_z|_{i-\frac{1}{2},j+\frac{1}{2},k}^{n+\frac{1}{2}} - H_z|_{i-\frac{1}{2},j-\frac{1}{2},k+1}^{n+\frac{1}{2}} - H_z|_{i-\frac{1}{2},j-\frac{1}{2},k}^{n+\frac{1}{2}}\Big)\end{aligned} \tag{23}$$

$$\begin{aligned}\left.\frac{\partial H_z}{\partial y}\right|_{i,j,k+\frac{1}{2}}^{n+\frac{1}{2}} = \frac{1}{4\Delta y}\Big(& H_z|_{i+\frac{1}{2},j+\frac{1}{2},k+1}^{n+\frac{1}{2}} + H_z|_{i+\frac{1}{2},j+\frac{1}{2},k}^{n+\frac{1}{2}} + H_z|_{i-\frac{1}{2},j+\frac{1}{2},k+1}^{n+\frac{1}{2}} + H_z|_{i-\frac{1}{2},j+\frac{1}{2},k}^{n+\frac{1}{2}} \\ & - H_z|_{i+\frac{1}{2},j-\frac{1}{2},k+1}^{n+\frac{1}{2}} - H_z|_{i+\frac{1}{2},j-\frac{1}{2},k}^{n+\frac{1}{2}} - H_z|_{i-\frac{1}{2},j-\frac{1}{2},k+1}^{n+\frac{1}{2}} - H_z|_{i-\frac{1}{2},j-\frac{1}{2},k}^{n+\frac{1}{2}}\Big)\end{aligned} \tag{24}$$

The remaining two derivatives, $\left.\frac{\partial H_x}{\partial y}\right|_{i,j,k+\frac{1}{2}}^{n+\frac{1}{2}}$ and $\left.\frac{\partial H_y}{\partial x}\right|_{i,j,k+\frac{1}{2}}^{n+\frac{1}{2}}$, are obtained in the usual manner directly from the FDTD grid. Using (16), (17), and (21)–(24) in (12) yields the complete expression for $E_z|_{i,j,k+\frac{1}{2}}^{n+1}$. Similar expressions can easily be obtained for E_x and E_y.

III. ONE-DIMENSIONAL CASE

The equations outlined in the previous section can be greatly simplified for a one-dimensional scatterer. In the remainder of this paper we will restrict spatial variation to the x-direction so that $\frac{\partial}{\partial y} = \frac{\partial}{\partial z} = 0$. The Yee cell then reduces to points along a line as shown in Fig. 2. Furthermore, we will assume that there is no coupling from the x component into the y and z components, and *vice versa*. Therefore, for a y- or z-polarized incident wave, there will be no x component of the electric and magnetic fields.

Using these assumptions, the magnetic field is given by

$$H_x|_i^{n+\frac{1}{2}} = 0 \tag{25}$$

$$H_y|_{i+\frac{1}{2}}^{n+\frac{1}{2}} = H_y|_{i+\frac{1}{2}}^{n-\frac{1}{2}} + \frac{\Delta t}{\mu_0 \Delta x}\left(E_z|_{i+1}^n - E_z|_i^n\right) \tag{26}$$

$$H_z|_{i+\frac{1}{2}}^{n+\frac{1}{2}} = H_z|_{i+\frac{1}{2}}^{n-\frac{1}{2}} - \frac{\Delta t}{\mu_0 \Delta x}\left(E_y|_{i+1}^n - E_y|_i^n\right) \tag{27}$$

and the electric field is given by

$$E_x|_{i+\frac{1}{2}}^{n+1} = 0 \tag{28}$$

$$\begin{aligned}E_y|_i^{n+1} = \frac{1}{\delta}\Bigg\{ & -\left(\frac{\epsilon_{xx}}{\Delta t} + \frac{\sigma_{xx}}{2}\right)\left(\frac{\epsilon_{yz}}{\Delta t} + \frac{\sigma_{yz}}{2}\right) \\ & \left[\left(\frac{\epsilon_{zy}}{\Delta t} - \frac{\sigma_{zy}}{2}\right) E_y|_i^n + \left(\frac{\epsilon_{zz}}{\Delta t} - \frac{\sigma_{zz}}{2}\right) E_z|_i^n + \frac{1}{\Delta x}\left(H_y|_{i+\frac{1}{2}}^{n+\frac{1}{2}} - H_y|_{i-\frac{1}{2}}^{n+\frac{1}{2}}\right)\right] \\ & + \left(\frac{\epsilon_{xx}}{\Delta t} + \frac{\sigma_{xx}}{2}\right)\left(\frac{\epsilon_{zz}}{\Delta t} + \frac{\sigma_{zz}}{2}\right) \\ & \left[\left(\frac{\epsilon_{yy}}{\Delta t} - \frac{\sigma_{yy}}{2}\right) E_y|_i^n + \left(\frac{\epsilon_{yz}}{\Delta t} - \frac{\sigma_{yz}}{2}\right) E_z|_i^n - \frac{1}{\Delta x}\left(H_z|_{i+\frac{1}{2}}^{n+\frac{1}{2}} - H_z|_{i-\frac{1}{2}}^{n+\frac{1}{2}}\right)\right]\Bigg\}\end{aligned} \tag{29}$$

$$\begin{aligned}E_z|_i^{n+1} = \frac{1}{\delta}\Bigg\{ & -\left(\frac{\epsilon_{xx}}{\Delta t} + \frac{\sigma_{xx}}{2}\right)\left(\frac{\epsilon_{zy}}{\Delta t} + \frac{\sigma_{zy}}{2}\right) \\ & \left[\left(\frac{\epsilon_{yy}}{\Delta t} - \frac{\sigma_{yy}}{2}\right) E_y|_i^n + \left(\frac{\epsilon_{yz}}{\Delta t} - \frac{\sigma_{yz}}{2}\right) E_z|_i^n - \frac{1}{\Delta x}\left(H_z|_{i+\frac{1}{2}}^{n+\frac{1}{2}} - H_z|_{i-\frac{1}{2}}^{n+\frac{1}{2}}\right)\right] \\ & + \left(\frac{\epsilon_{xx}}{\Delta t} + \frac{\sigma_{xx}}{2}\right)\left(\frac{\epsilon_{yy}}{\Delta t} + \frac{\sigma_{yy}}{2}\right) \\ & \left[\left(\frac{\epsilon_{zy}}{\Delta t} - \frac{\sigma_{zy}}{2}\right) E_y|_i^n + \left(\frac{\epsilon_{zz}}{\Delta t} - \frac{\sigma_{zz}}{2}\right) E_z|_i^n + \frac{1}{\Delta x}\left(H_y|_{i+\frac{1}{2}}^{n+\frac{1}{2}} - H_y|_{i-\frac{1}{2}}^{n+\frac{1}{2}}\right)\right]\Bigg\}\end{aligned} \tag{30}$$

where δ is still the determinant of $\left(\frac{1}{\Delta t}\overline{\overline{\epsilon}} + \frac{1}{2}\overline{\overline{\sigma}}\right)$. Note that these equations are only marginally more complicated than the isotropic FDTD equations.

TABLE I
MATERIAL PARAMETERS.

Layer	Thickness	Permeability	Permittivity	Conductivity S/m
1	3.75 mm	μ_0	$43\epsilon_0$	$\begin{pmatrix} 0.0 & 0.0 & 0.0 \\ 0.0 & 12.0 & 0.0 \\ 0.0 & 0.0 & 0.0 \end{pmatrix}$
2	3.75 mm	μ_0	$43\epsilon_0$	$\begin{pmatrix} 0.0 & 0.0 & 0.0 \\ 0.0 & 8.5 & 8.5 \\ 0.0 & 8.5 & 8.5 \end{pmatrix}$
3	3.75 mm	μ_0	$43\epsilon_0$	$\begin{pmatrix} 0.0 & 0.0 & 0.0 \\ 0.0 & 0.0 & 0.0 \\ 0.0 & 0.0 & 12.0 \end{pmatrix}$

The permeability and permittivity of the sample are isotropic while the conductivity is anisotropic. The ordering of the elements in the conductivity tensor is the same as in (1).

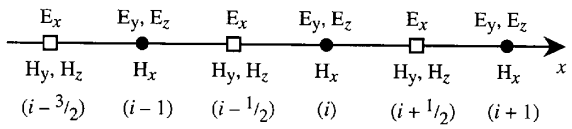

Fig. 2. The Yee cell reduced to one dimension.

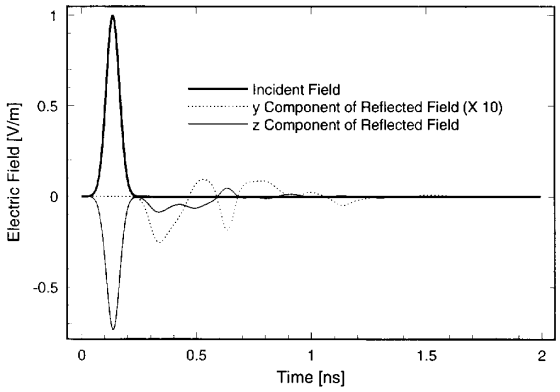

Fig. 3. The z-polarized incident field and the reflected fields. The y component of the reflected field has been scaled by a factor of 10.

IV. RESULTS FOR ONE-DIMENSIONAL CASE

To demonstrate the capability of the anisotropic FDTD algorithm, we will consider a layered material that consists of three slabs of anisotropic material. The parameters chosen for this example are based on those of an actual carbon fiber composite material used in modern aircraft. In each layer, we will assume the conductivity is high in the direction parallel to the fibers and negligible in the perpendicular direction. It is also assumed that the fiber orientation in each layer is rotated by 45° relative to the preceding layer. It is further assumed that the only variation is in the x direction; i.e., the planar boundaries between layers are perpendicular to the x axis. The specific parameters for this case are given in Table I. These values indicate that the fibers are parallel to the y direction in the first layer and parallel to the z direction in the third. In the second layer, the fiber orientation forms a 45° angle with both the y and z axes. The permittivity and permeability are isotropic.

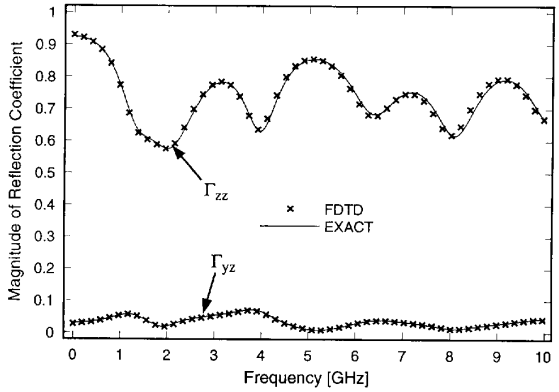

Fig. 4. The magnitude of the reflection coefficients as a function of frequency.

Owing to the anisotropic conductivity of this material, a z-polarized incident wave will produce a scattered field with both y and z components. Thus, for a z-polarized incident wave, we must define the reflection coefficient Γ_{zz}, which is the ratio of the z component of the scattered field to the z component of the incident field, and the reflection coefficient Γ_{yz}, which is the ratio of the y component of the scattered field to the z component of the incident field. Using the FDTD equations given in Section III, the fields reflected from this material sample can be easily calculated. Furthermore, by illuminating the material with a pulse and recording the transient incident and scattered fields, the frequency dependence of the reflection coefficients can be determined through the use of Fourier transforms.

Fig. 3 shows the incident z-polarized wave that was used to illuminate the sample described in Table I. This is a Gaussian pulse that falls off to one ten-thousandth of the peak value after 800 time steps and each time step, Δt, is 156.25 fs. The spatial step size, Δx, used in the FDTD calculation was 93.75 μm so that each layer was $40\Delta x$ thick. Fig. 3 also shows the z component of the reflected field obtained from the anisotropic FDTD code. For the sake of clarity, the y component of the reflected field in Fig. 3 has been multiplied by a factor of 10; i.e., actual values are one-tenth those shown in the figure.

Using the permittivity and conductivity tensors for a given layer of anisotropic material, one can calculate the propagation constants and polarizations of the two eigenmodes of plane-wave propagation [13].

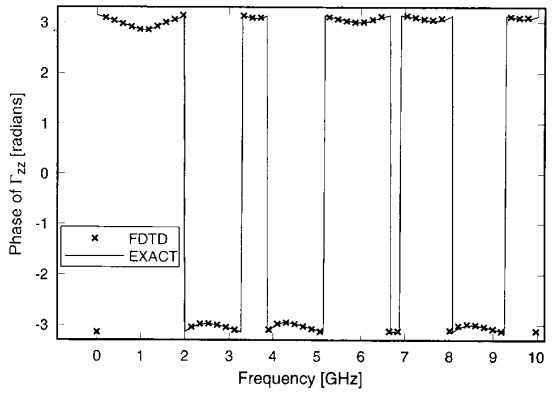

(a)

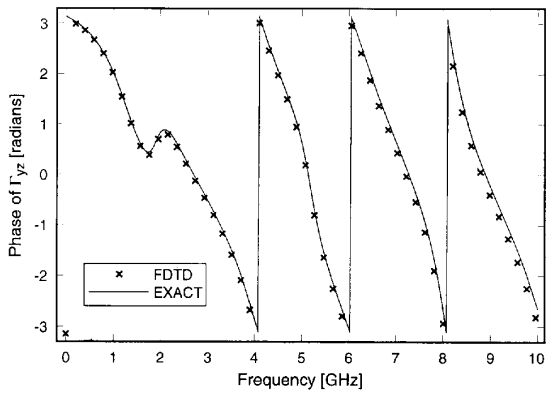

(b)

Fig. 5. The phase of the reflection coefficients as a function of frequency. (a) Γ_{zz}. (b) Γ_{yz}.

Expanding both the $+x$ and $-x$ traveling components of the field in terms of these eigenmodes and requiring continuity of tangential field components at each interface, we arrive at a linear system which can be solved to give the exact reflection coefficients Γ_{zz} and Γ_{yz}.

Fourier transforming the temporal signals shown in Fig. 3 and then normalizing the reflected field transforms by the incident field transform yields the spectral description of the reflection coefficients. Fig. 4 shows the exact and FDTD-obtained values of the magnitude of Γ_{zz} and Γ_{yz}. The FDTD computation was performed over 32 768 time steps to yield a frequency resolution of approximately 195.3 MHz. Fig. 4 shows excellent agreement between the two results. There is a slight offset between the FDTD and exact analytic results at higher frequencies, which can be attributed to the inherent dispersion in the FDTD algorithm [3]. Fig. 5 shows the phase of Γ_{zz} and Γ_{yz} obtained from FDTD and the exact analytic formulation. Again, excellent agreement is seen and the only difference is a slight offset that occurs at higher frequencies.

Many other trials using different material parameters were run to further compare the FDTD and analytic results. The two methods consistently showed agreement as good as that shown in Figs. 4 and 5.

V. Conclusions

We have extended the FDTD algorithm to accommodate nonzero off-diagonal elements in the permittivity and conductivity tensors. This permits the study of a much broader class of materials than was previously possible. Excellent agreement is obtained between an exact analytic method and the anisotropic FDTD algorithm for a one-dimensional scatterer. Although the traditional FDTD algorithm can accommodate anisotropic materials, it is restricted to anisotropies that produce diagonal tensors. For diagonal tensors, the resulting equations are substantially unchanged from those originally used by Yee. However, many situations can arise, such as the example considered in this paper, where the tensors cannot be diagonalized. Therefore, the extensions provided here become essential for any FDTD analysis of general anisotropic materials.

References

[1] K. Yee, "Numerical solution of initial boundary value problems involving Maxwell's equations in isotropic media," *IEEE Trans. Antennas Propogat.*, vol. 14, pp. 302–307, 1966.

[2] A. Taflove and M. E. Brodwin, "Numerical solution of steady-state electromagnetic scattering problems using the time-dependent Maxwell's equations," *IEEE Trans. Microwave Theory Tech.*, vol. 23, no. 8, pp. 623–630, 1975.

[3] A. Taflove, "Review of the formulation and applications of the finite-difference time-domain method for numerical modeling of electromagnetic wave interactions with arbitrary structures," *Wave Motion*, vol. 10, pp. 547–582, 1988.

[4] G. Mur, "Absorbing boundary conditions for the finite-difference approximation of the time-domain electromagnetic-field equations," *IEEE Trans. Electromagn. Compat.*, vol. 23, no. 4, pp. 377–382, 1981.

[5] Z. Liao, H. Wong, B. Yang, and Y. Yuan, "A transmitting boundary for transient wave analyses," *Scientia Sinica A*, vol. 27, no. 10, pp. 1063–1076, 1984.

[6] W. Chew, *Waves and Fields in Inhomogeneous Media*. New York: Van Nostrand Reinhold, 1990, pp. 251–256.

[7] R.J. Luebbers, F. Hunsberger, K. S. Kunz, R. B. Standler, and M. Schneider, "A frequency-dependent finite-difference time-domain formulation for dispersive materials," *IEEE Trans. Electromagn. Compat.*, vol. 32, no. 3, pp. 222–227, 1990.

[8] R. J. Luebbers, F. Hunsberger, and K. S. Kunz, "A frequency-dependent finite-difference time-domain formulation for transient propagation in plasma," *IEEE Trans. Antennas Propagat.*, vol. 39, no. 1, pp. 29–34, 1991.

[9] L. J. Nickisch and P. M. Franke, "Finite-difference time-domain solution of Maxwell's equations for the dispersive ionosphere," *IEEE Antennas Propagat. Magazine*, vol. 34, no. 5, pp. 33–39, 1992.

[10] A. Taflove and K. R. Umashankar, "Analytic models for electromagnetic scattering," Final Report RADC-TR-85-87 on contract F19 628-82-C-0104, Electromagn. Sci. Div., Rome Air Dev. Center, Hanscom AFB, MA, 1985.

[11] B. Beker, K. R. Umashankar, and A. Taflove, "Numerical analysis and validation of the combined field surface integral equations for electromagnetic scattering by arbitrary shaped two-dimensional anisotropic objects," *IEEE Trans. Antennas Propagat.*, vol. 37, no. 12, pp. 1573–1581, 1989.

[12] M. A. Strickel and A. Taflove, "Time-domain synthesis of broadband absorptive coatings for two-dimensional conducting targets," *IEEE Trans. Antennas Propagat.*, vol. 38, no. 7, pp. 1084–1091, 1990.

[13] A. Yariv and P. Yeh, *Optical Waves in Crystals*. New York: Wiley, 1984.